

autoTICI: Automatic Brain Tissue Reperfusion Scoring on 2D DSA Images of Acute Ischemic Stroke Patients

Ruisheng Su, Sandra A.P. Cornelissen, Matthijs van der Sluijs, Adriaan C.G.M. van Es, Wim H. van Zwam, Diederik W.J. Dippel, Geert Lycklama, Pieter Jan van Doormaal, Wiro J. Niessen, Aad van der Lugt, and Theo van Walsum

Abstract—Thrombolysis in Cerebral Infarction (TICI) score is an important metric for reperfusion therapy assessment in acute ischemic stroke. It is commonly used as a technical outcome measure after endovascular treatment (EVT). Existing TICI scores are defined in coarse ordinal grades based on visual inspection, leading to inter- and intra-observer variations. In this work, we present autoTICI, an automatic and quantitative TICI scoring method. First, each digital subtraction angiography (DSA) sequence is separated into four phases (non-contrast, arterial, parenchymal and venous phase) using a multi-path convolutional neural network (CNN), which exploits spatio-temporal features. The network also incorporates sequence level label dependencies in the form of a state-transition matrix. Next, a minimum intensity map (MINIP) is computed using the motion corrected arterial and parenchymal frames. On the MINIP image, vessel, perfusion and background pixels are segmented. Finally, we quantify the autoTICI score as the ratio of reperfused pixels after EVT. On a routinely acquired multi-center dataset, the proposed autoTICI shows good correlation with the extended TICI (eTICI) reference with an average area under the curve (AUC) score of 0.81. The AUC score is 0.90 with respect to the dichotomized eTICI. In terms of clinical outcome prediction, we demonstrate that autoTICI is overall comparable to

eTICI.

Index Terms—Stroke, DSA, autoTICI, Deep Learning, Brain Tissue Perfusion, Phase Classification, MR CLEAN Registry

I. INTRODUCTION

A. Clinical Background

STROKE remains one of the worldwide leading causes of death and serious long-term disability [1]. Due to the ageing population, stroke incidence is rising, which is posing a large and still increasing public health burden to the society. Ischemic stroke, which is caused by an occluded artery of the brain, is the most common stroke type, accounting for about 88% of all strokes [2].

Recent studies have shown that endovascular thrombectomy (EVT) improves outcome in patients with acute ischemic stroke caused by a large vessel occlusion (LVO) in the anterior circulation [3], [4]. This led to novel studies on maximizing patient benefits before and during EVT. Many studies have focused on pre-interventional patient selection and outcome prediction based on scores such as Alberta Stroke Program Early CT Score (ASPECTS) [5] and collateral score [6]. A recent study [7] demonstrated that peri-procedural imaging data can be valuable for predicting treatment outcome, which can in turn assist interventionalists to achieve better treatment quality.

DSA is the imaging modality to guide the EVT procedure. Despite rapid research progress in computational stroke related biomarker extraction from computed tomographic angiography (CTA) [8] and CT Perfusion (CTP) [9] images, automatic peri-procedural imaging biomarker extraction from DSA is yet to be further explored.

One of the most widely adopted metrics for evaluation of EVT quality and prediction of functional outcome on DSA images is the so-called Thrombolysis In Cerebral Infarction (TICI) score [2] and its variants, such as modified TICI (mTICI) [10], extended TICI (eTICI) [11] and expanded TICI [12]. The TICI scores define the extent of brain reperfusion. For example, the eTICI score is defined as follows:

- **eTICI 0**: no perfusion or antegrade flow in the target downstream territory (TDT). TDT refers to the occluded

The MR CLEAN Registry was partly funded by TWIN Foundation, Erasmus MC University Medical Center, Maastricht University Medical Center, and Amsterdam University Medical Centers. The current work was financially supported by Health-Holland (TKI Life Sciences and Health), Q-Maestro project (grant number: EMCLSH19006) and Philips Healthcare (Best, The Netherlands).

R. Su and T. van Walsum are with the Biomedical Imaging Group Rotterdam, Department of Radiology & Nuclear Medicine, Erasmus MC, University Medical Center Rotterdam, The Netherlands (e-mail: r.su@erasmusmc.nl).

S.A.P. Cornelissen, M. van der Sluijs, P.-J. van Doormaal and A. van der Lugt are with the Department of Radiology & Nuclear Medicine, Erasmus MC, University Medical Center Rotterdam, The Netherlands.

A.C.G.M. van Es is with the Department of Radiology, Leiden UMC, Leiden, The Netherlands.

W.H. van Zwam is with the Department of Radiology & Nuclear Medicine, Maastricht UMC, Cardiovascular Research Institute Maastricht, The Netherlands.

D.W.J. Dippel is with the Department of Neurology, Erasmus MC, University Medical Center Rotterdam, The Netherlands.

G. Lycklama is with the Department of Radiology, Haaglanden Medical Center, The Hague, The Netherlands.

W.J. Niessen is with the Biomedical Imaging Group Rotterdam, Department of Radiology & Nuclear Medicine, Erasmus MC, University Medical Center Rotterdam, The Netherlands, and with the Faculty of Applied Sciences, Delft University of Technology, The Netherlands.

brain region that was supplied via antegrade blood flow prior to stroke onset [13];

- **eTICI 1:** blood flow past initial site of occlusion, but with minimal brain tissue perfusion;
- **eTICI 2A:** perfusion of $\leq 50\%$ of TDT;
- **eTICI 2B:** perfusion of $\geq 50\%$ of TDT;
- **eTICI 2C:** nearly complete perfusion except for slow flow or presence of small emboli in distal cortical vessels;
- **eTICI 3:** complete perfusion.

Above TICI score variants were introduced as attempts towards standardizing EVT treatment success scoring. However, these grading metrics suffer from several shortcomings:

- Inter- and intra-observer variation: TICI assessment by visual inspection is inherently error prone, as it is subject to various factors, such as experience level of the rater and inspection attentiveness. Moreover, a recent study showed that TICI scores are generally overestimated by operators during EVT compared to core-lab raters [14];
- Coarse ordinal scale: TICI-like scores are mostly defined in 4-6 grades. Several studies have indicated that EVT outcome is associated with greater degrees of reperfusion [15]–[19]. More granular perfusion grading systems would probably help to better assess treatment success;
- Conceptual confusion: in EVT terms, reperfusion is the antegrade restoration of a capillary blush, whereas recanalization generally refers to the restoration of blood flow past the arterial occlusion [13]. In other words, recanalization is a necessary but insufficient condition for reperfusion. Although TICI scores define reperfusion scales, the concept of recanalization and reperfusion is often interchanged during visual TICI assessment in clinical practice [13]. As a result, the cases of successful recanalization without adequate brain tissue reperfusion are usually overlooked, leading to overestimated TICI.

To mitigate the above limitations of existing TICI scoring mechanisms, we pursue objective, robust and quantitative TICI scoring in a fully automated manner.

B. Related Work

In recent years, the field of computer vision evolved rapidly. Triggered by the advances in deep learning particularly, automated medical imaging analysis has gained momentum as well. In the field of stroke imaging, various algorithms on automatic quantification of imaging biomarkers have been proposed lately. These algorithms can be categorized into two groups based on the target imaging modality: pre-treatment imaging and peri-procedural imaging.

For pre-treatment prognosis, MRI, CTA and CTP images are widely used. Robben *et al.* [9] exploited a multi-path CNN to predict the final infarct volume from CTP images and treatment metadata. Nielsen *et al.* [20] demonstrated state-of-the-art performance of a deep CNN on final lesion volume and treatment outcome prediction on MRI images. Su *et al.* [8] utilized a U-Net architecture to quantify collateral scores from 3D CTA images. Related to brain perfusion estimation, McKinley *et al.* [21] developed an automated pipeline for

penumbra volume estimation based on random forests using multi-modal MRI.

For peri-procedural evaluation of treatment effect, DSA is still considered the standard modality. Automatically quantified biomarkers on DSA have received less attention. As an example, Liebeskind *et al.* [22] recently proposed a machine learning based automatic arterial input function (AIF) extraction method. Concerning TICI scoring on DSA, to the best of our knowledge, no fully automatic algorithm has been proposed yet. Nevertheless, Prasetya *et al.* [23] recently developed a quantitative TICI (qTICI) scoring pipeline which demands manual annotation. First, given a DSA sequence under assessment, venous phase frames need to be manually removed by a neuro/interventional radiologist so to exclude the retrograde perfusion (via pial collaterals), as only antegrade (via recanalization) perfusion defines the reperfusion. Second, an estimated TDT is delineated by an expert observer for each artery occlusion of the DSA under assessment. Lastly, qTICI is defined as the percentage of reperfused pixels within TDT based on a threshold relative to the maximum intensity. Prasetya *et al.* [23] demonstrated reliable correlation between qTICI and eTICI, revealing the potential value of quantitative TICI as an objective biomarker. Nevertheless, as qTICI relies on a series of manual steps, such a semi-automatic approach is more time consuming than traditional TICI grading procedures in practice. In addition, these manual steps are inevitably subjective, which can introduce new factors to inter- and intra-observer variability.

Beyond qTICI, we seek a fully automatic, yet explainable step by step approach for quantitative TICI scoring.

C. Contributions

The main contribution of this work is two-fold:

- we propose a fully automatic and quantitative TICI scoring algorithm, as an objective and robust alternative to existing visual inspection based TICI scoring;
- we assess the proposed methods on a large multi-center data set acquired in clinical routine.

The remainder of this paper is organized as follows: Section II provides a detailed overview of our proposed methods and Section III describes the data used for experiments. Section IV presents the experiment results and performance evaluations of the proposed methods, followed by further discussions in Section V. Finally, Section VI concludes the paper.

II. METHOD

Existing TICI scores are visually graded by estimating the extent of brain tissue-level reperfusion (post-EVT, numerator) in the initial TDT (pre-EVT, denominator). This would require a visual comparison between pre- and post-EVT sequences. Following this definition and the visual TICI scoring principles, we propose to automatically extract the numerator and denominator for quantitative TICI scoring.

As illustrated in Fig. 1, the proposed algorithm comprises four components: phase separation, motion correction, perfusion segmentation and TICI scoring. First, given four DSA

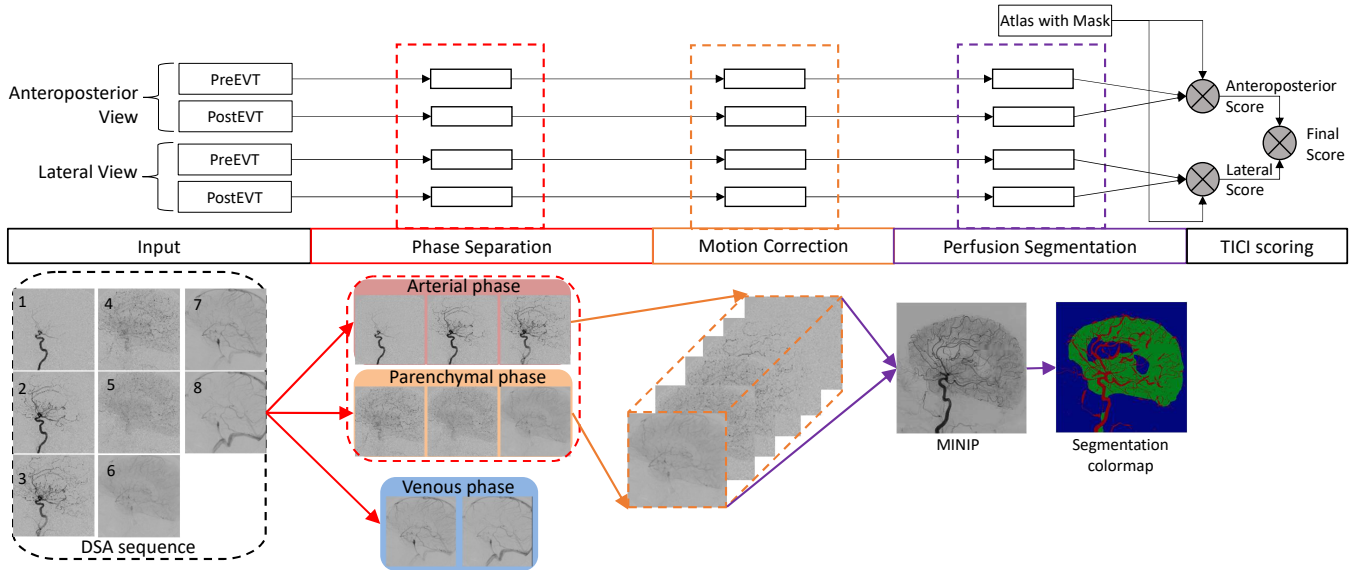


Fig. 1: Proposed pipeline for automatic TIC1 scoring.

sequences for each patient, both anteroposterior (AP) and lateral views for both pre-EVT and post-EVT, each of these sequences is separated into four phases, being non-contrast, arterial, parenchymal and venous phase. We trained a multi-channel CNN model to label image phases based on spatio-temporal textural features, as well as sequence label transition rules. Subsequently, venous phase frames are removed from the sequence. Non-contrast frames are also excluded, as they contain no valid information, but merely motion artifacts. The remaining sequence frames are aligned based on affine registration to correct motion artifacts. Third, a single 2D minimum intensity map (MINIP) is calculated from the aligned sequence, which is then segmented into vessels, perfused area and non-perfused (including background) area. Finally, by comparing the perfusion area before and after EVT treatment, a quantitative TIC1 score is deduced as the percentage of re-perfused area out of previously occluded downstream territory. Each of the components is further detailed below.

A. Phase Classification

The purpose of the phase classification step is to recognize and separate the venous phase frames; these frames need to be excluded from the series, because these may contain late perfusion attributed to retrograde flow via pial collaterals.

Existing phase separation methods can be grouped into two types: supervised and unsupervised. Lee *et al.* [24] used the independent component analysis (ICA) technique to separate a DSA sequence into three images (arterial, parenchymal and venous). Such unsupervised methods rely on the assumption of expected number of components. For supervised methods, Schuldhaus *et al.* [25] utilized Rosenblatt perceptron-based classification using handcrafted positional intensity features.

In this work, we propose a CNN based method for automatic phase separation. An overview of the framework is shown in Fig. 2. Provided a DSA sequence, a pretrained ResNet18 takes each frame together with its direct neighbors as input and predicts a phase label. Next, on the sequence level, a

tailored state-transition diagram is applied on the predicted label probabilities to ensure a logical label sequence based on maximum likelihood.

1) *Phase Definition*: A complete run of a DSA sequence can be categorized into three phases based on the blood flow: the arterial, parenchymal and venous phase. Fig. 3 shows an example of each phase in AP and lateral views. In practice, the first or last few frames generally have no visible contrast. In this work, we consider non-contrast as an additional phase. The phases were defined according to the following criteria (determined by a clinical expert):

- Arterial phase:
 - First frame: appearance of contrast in image;
 - Last frame: appearance of contrast in cortical arterial branches. These are the peripherally located arterial branches which run on the cortex of the brain;
- Parenchymal phase:
 - Last frame: right before appearance of contrast in the superior sagittal sinus (SSS);
- Venous phase:
 - First frame: appearance of contrast in the SSS;
 - Last frame: the last frame with clearly visible contrast thereafter.

It should be noted that a complete run of DSA does not necessarily contain all four phases. Whether these phases are all present depends on the level of the occlusion, the timing of the acquisition with respect to the contrast injection and the frame rate. In case of a carotid-T occlusion, mostly only an arterial phase is present because no contrast penetrates the affected hemisphere from the vessel where contrast was injected, and in some short acquisitions, the venous phase may not be present.

2) *Network Architecture*: The proposed network architecture is shown in Fig. 2. The network is based on ResNet-18 proposed by He *et al.* [26], to which we made modifications to adapt it to our task. In our case, the input is set to three

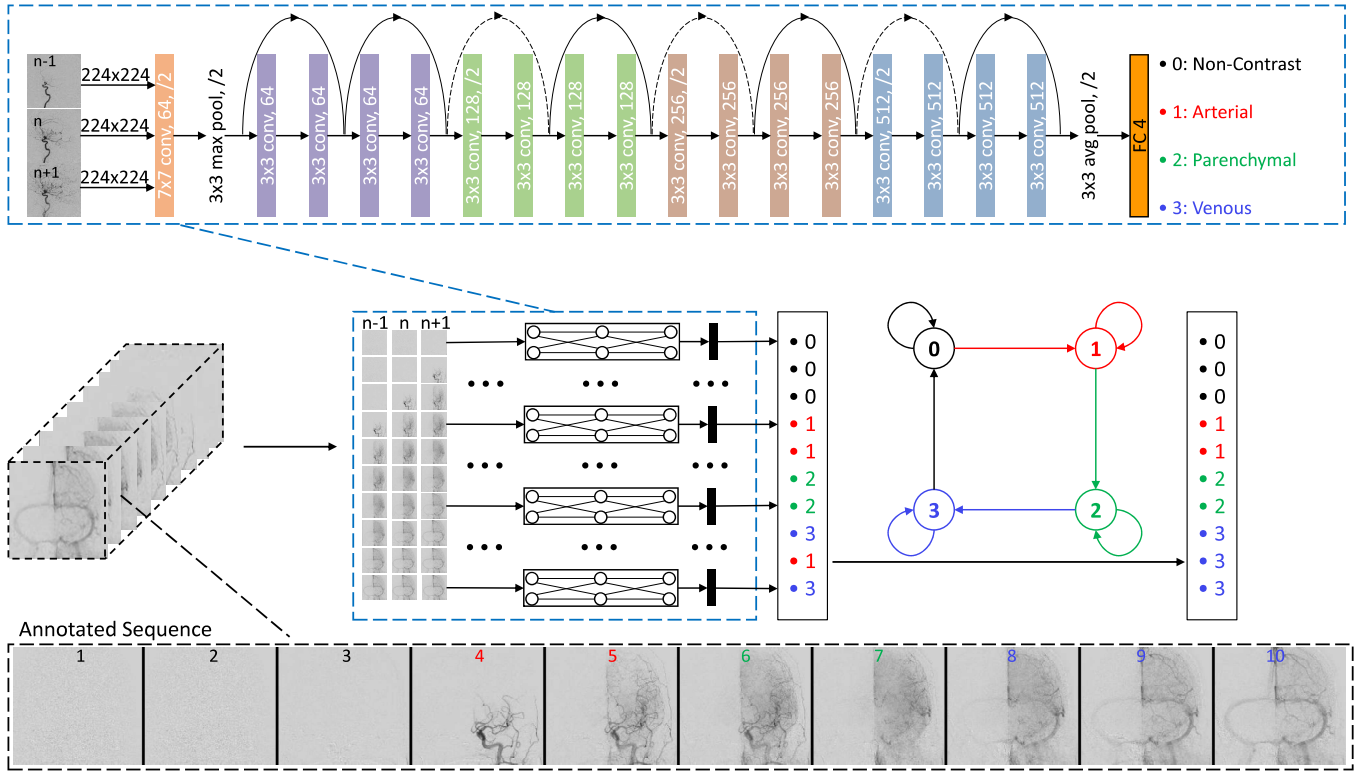


Fig. 2: An overview of the phase classification framework.

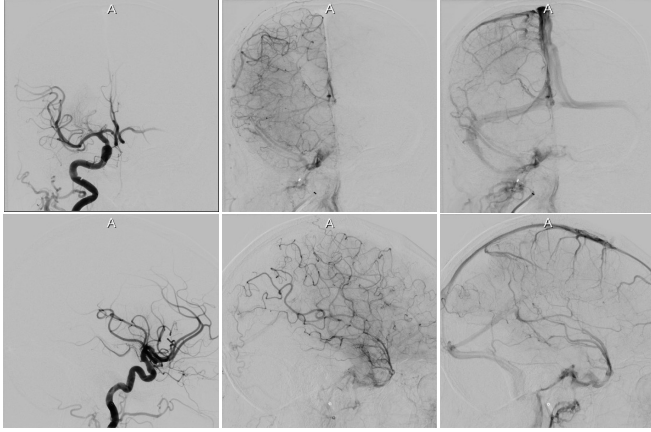


Fig. 3: DSA examples of arterial (left column), parenchymal (middle column) and venous (right column) phases. Top row: frontal view; bottom row: AP view.

consecutive 2D sequence frames, each for one input channel. In such a way, local features of three consecutive frames are fused. Our network ends with a fully connected (FC) layer with softmax normalization, which outputs an array of four elements with predicted per-phase probabilities.

3) Constrained Sequence Labelling: On the sequence level, a handcrafted state transition diagram (see Fig. 2) is applied to suppress invalid phase transitions from frame to frame. The rationale is that although the network fuses neighboring frames which possess temporal contrast flow information, the global sequence level information is not fully exploited. For instance, in a correctly ordered sequence, no arterial phase

should appear during or after parenchymal phase. All sequence labels should follow a certain state transition logic. We embed this logic to bring further robustness to the network.

Conditional Random Fields (CRFs) [27] are a popular type of undirected probabilistic models that can be used to implement sequential dependencies in machine learning tasks, especially in labeling or parsing of sequential data. CRFs train a transition matrix between previous and current labels by maximum likelihood learning. At the inference step, the transition matrix, a set of numerical weights, is applied on the sequence label probabilities to obtain the most likely overall label path using the Viterbi algorithm [28].

In this work, we adopted the idea of conditional random field and tailored it according to our task. Instead of training the conditional dependency between frames in a data-driven manner, we handcrafted the structural logic between labels directly into a transition matrix. The state transition diagram in Fig. 2 shows the allowed transitions between phases, which translates to the following transition matrix, where all allowed transitions are denoted as $T_{i,j} = 1$:

$$T = \begin{pmatrix} 1 & 1 & 0 & 0 \\ 0 & 1 & 1 & 0 \\ 0 & 0 & 1 & 1 \\ 1 & 0 & 0 & 1 \end{pmatrix}. \quad (1)$$

We intentionally assigned equal weights to all allowed transitions ($T_{i,j} = 1$) to avoid bias introduced by the training data itself. The remaining decoding and inference steps were kept the same as in CRF.

After phase classification, only arterial and parenchymal phase frames are carried on for further processing. Fig. 4

shows an example of the venous phase removal effect.



Fig. 4: A MINIP before (a) and after (b) venous phase removal.

B. Motion Corrected MINIP

The image segmentation and quantification steps rely on the MINIP, which is a 2D image with each pixel being its minimum intensity value (which reflects the attenuation caused by iodine contrast agent) across the time axis of the sequence. Patient movements (voluntary or involuntary) during image acquisition may hamper this quantification, as they may cause vessels to be less apparent, and to overlap with brain tissue in the MINIP image. Therefore, the purpose of motion correction is to correct frame misalignments introduced by patient motion during image acquisition.

In this work, we used an affine registration that optimizes the Mattes mutual information [29]. Fig. 5 visualizes the sequence motion compensation on the calculated MINIP image.

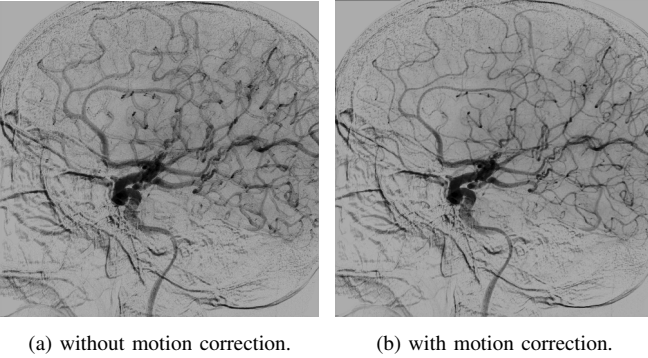


Fig. 5: A MINIP image without (a) and with (b) motion correction.

C. Perfusion Segmentation

The result of the previous steps is a MINIP of the motion corrected DSA sequence, that only contains arterial and parenchymal phases. From the constructed 2D MINIP image, (see Fig. 1), we segment blood vessels and perfused area from the image background, which serves as a prerequisite for the subsequent (re-)perfusion quantification. Firstly, the contrast-opacified blood vessels are segmented using the multi-scale vesselness Frangi filter [30]. We opted for such a proven vessel segmentation approach instead of deep learning methods, as we do not rely on high precision vessel segmentation, rather

we exclude the vessel pixels such that perfusion area can be better segmented. Such a traditional algorithm satisfied our needs. Next, the remaining pixels are automatically clustered into two groups, perfused and non-perfused (including background), using Otsu's thresholding technique [31], which is an effective and parameter free method based on the image intensity histogram. Image background is included in the histogram so that perfused pixels can be recognized. Finally, a segmentation colormap is constructed (see Fig. 1), where vessels, perfused and non-perfused pixels are represented in red, green and blue respectively.

D. TICI Quantification

Finally, a quantitative TICI score can be computed from the resulted segmentation colormap. Both AP and lateral views are evaluated. Traditional visual TICI-like scores assess the change in the level of perfusion after EVT with respect to pre-EVT. Similarly, the proposed autoTICI score quantifies the ratio of re-perfused area versus the initial TDT, which can be formulated as follows:

$$\text{autoTICI} = \frac{TDT_{preEVT} \cap P_{postEVT}}{TDT_{preEVT}}, \quad (2)$$

where $P_{postEVT}$ denotes perfused pixels after EVT (green and orange area in Fig. 6c) and TDT_{preEVT} is the initially occluded brain area prior to EVT (white area in Fig. 6). While $P_{postEVT}$ is available in the segmentation colormap, the distinction between non-perfused pixels and pure image background in the pre-EVT image is yet to be made. To this end, we introduce an atlas-based approach to exclude the out-of-skull pixels. More specifically, we utilize masked DSA atlases to align the brain area from atlas to the post-EVT MINIP of patients. 22 DSA sequences were selected as atlases from patients without stroke (Section III-B.5). We apply affine registration (similar to the registration used in motion correction in Section II-B) to spatially align the atlases with the post-EVT image. The final registered atlas for each subject is the one with the maximum Mattes mutual information [29]. The pre-EVT MINIP is also registered to post-EVT MINIP. In such a way, the brain region mask on the registered atlas can be mapped to pre- and post-EVT MINIP. TDT_{preEVT} and $P_{postEVT}$ are determined within the aligned brain mask. As illustrated in Fig. 6, autoTICI represents the ratio of reperfused pixels (orange area) versus the pre-EVT TDT (white area).

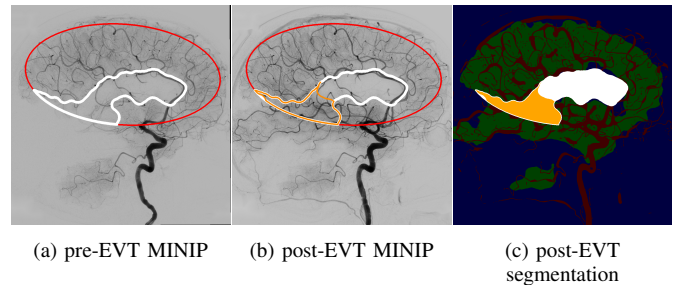


Fig. 6: An example of TICI quantification. Red: brain mask; white: TDT_{preEVT} ; orange: reperfused area ($TDT_{preEVT} \cap P_{postEVT}$).

III. DATA AND ANNOTATION

A. Data Selection

In this work, we used the MR CLEAN Registry [32] dataset for training and evaluating the proposed methods. The MR CLEAN Registry is an on-going multi-center registry which contains all patients with acute ischemic stroke who underwent EVT in the Netherlands since March 2014 [32]. Due to the large variety in acquisition systems and imaging protocols in different centers as well as differences in patient condition, the acquired DSA images possess great variability in image appearance and quality. Therefore, it is necessary to perform data selection in order to obtain a set of qualified yet representative data for our study.

1) *Phase Classification Dataset*: For training and evaluating the proposed phase separation algorithm, the following selection criteria were applied:

- **Sequence length**: due to non-uniformed data collection procedures across intervention centers, not all DSA sequences were collected in the format of a sequence; often only a few snapshots were stored. Moreover, we expect a qualified image sequence to contain most of the contrast flow. Based on our observation, sequences with less than six frames are insufficient for our purpose, thus excluded;
- **Image quality**: for the data to be usable, a number of quality criteria must be met: (i) the sequence must be a cerebral DSA; (ii) the sequence must possess sufficiently visible amount of contrast; (iii) the sequence should not exhibit substantial motion artifacts, such as motion blur, which is not trivial to eliminate via post-processing;
- **Occlusion location**: in this study, we consider patients that had an occlusion of the intracranial internal carotid artery (ICA) or the M1 segment, as these are the most common indications for EVT.

The MR CLEAN Registry (part 1) contains 1488 patients, which were collected from March 16, 2014 till June 15, 2016. DSA sequences were stored for 1479 patients, out of which 987 patients had an occlusion of either ICA or M1. After removing all short sequences (less than six frames), 872 patients remained. Subsequently, 192 patients were excluded during to lack of good quality image sequences, which led to 680 qualified patients. From each of those, we selected up to four sequences (pre-EVT/post-EVT, AP/lateral view) per subject which were of good image quality as described above.

For the purpose of phase classification, we ended up with 680 qualified patients, 1857 sequences and 30297 images. Non-subtracted, duplicated, inverted, corrupted frames were removed and finally all sequences were re-ordered according to frame acquisition time.

From the aforementioned qualified patients, a subset of 141 patients was suitable for TICI quantification (See next section for more details, Section III-A.2), this subset was fully annotated and used for testing in phase classification (and thus excluded from the set of training images). From the remaining 539 patients, 648 sequences (9440 images) were randomly selected (to limit the number of images to annotate), on which the proposed algorithm was trained and evaluated via cross validation.

TABLE I: eTICI and mRS score distribution on 141 test patients.

Training set: 539 patients, 648 sequences, 9440 images					
Test set: 141 patients, 564 sequences, 7421 images					
Statistics on test set					
post-EVT eTICI	Number of patients		mRS score		Number of patients
0	14	(9%)	favorable	0 (no symptoms)	6 (4%)
1	4	(2%)		1	20 (14%)
2A	24	(17%)		2	37 (26%)
2B	27	(19%)	unfavorable	3	18 (12%)
2C	22	(15%)		4	12 (8%)
3	50	(35%)		5	6 (4%)
				6 (death)	42 (29%)

2) *TICI Quantification Dataset*: To obtain a qualified DSA dataset for TICI quantification experiments and the overall algorithm evaluation, we applied further data selection criteria on top of the selected dataset for phase classification as follows:

- **Reference eTICI score**: in this study, eTICI score was used as the reference standard for evaluating the proposed autoTICI. Therefore, it is required that both pre-EVT and post-EVT sequences were scored. In addition, a pre-EVT eTICI score of 2 or higher indicates that the occlusion has been reopened before EVT treatment, thus these images were excluded for further analysis;
- **Four sequence per patient**: in order to investigate the sensitivity of autoTICI on both AP and lateral views, pre-EVT and post-EVT DSA sequences for both views should be available;
- **Image quality**: for accurate TICI quantification, the acquired image sequence should fulfill the following image quality criteria: (i) TDT of the brain should be fully visible in the image view; (ii) the view of the sequence should not be substantially rotated. As our DSA images are 2D projections of the brain, affine transformations are unable to fix 3D rotation artifacts in its 2D projects.

Out of the 680 qualified patients from the previous selection, 34 patients were excluded due to no valid eTICI score. Following it, image quality criteria were applied and patients with four sequences available were selected, which leads to 141 patients (564 sequences) for TICI quantification and testing of phase classification. The statistics of selected patient information is summarized in Table I.

B. Data Annotation

1) *TICI Score Reference Standard*: In the MR CLEAN registry, the eTICI [11] was visually scored by independent core-lab neuroradiologists. In this work, we compared the proposed autoTICI against eTICI.

2) *Modified Rankin Scale (mRS)*: The mRS score assesses the neurological independence of patients at day 90 following an EVT. It is a seven-grade scale, running from no symptoms (score: 0) to death (score: 6). In this study, we used the mRS score as a reference to evaluate the outcome predictability of the proposed autoTICI. Table I describes the mRS score

distribution on the test data set. Note that 20 patients had missing mRS records, which were imputed using multiple imputations by chained equations (MICE) [33]. We dichotomized the mRS scores to indicate favorable and unfavorable treatment outcomes.

3) *National Institutes of Health Stroke Scale (NIHSS)*: NIHSS quantifies the impairment of stroke patients by evaluating 11 aspects. It is an ordinal score ranging from 0 (no symptoms) to a maximum of 42. In MR CLEAN registry, both the baseline (prior to EVT, $NIHSS_{BL}$) and follow-up (within 24 hours after EVT, $NIHSS_{FU}$) scores were assessed. In our experiments, we derived the NIHSS shift as follows:

$$NIHSS_{shift} = NIHSS_{BL} - NIHSS_{FU} \quad . \quad (3)$$

4) *Sequence Phase Labelling*: Manual phase labelling was performed independently by three annotators, one experienced clinician, one colleague researcher and the first author, using an in-house developed tool in MevisLab. According to the phase definition (Section II-A.1), the sequence labelling output is a per frame label sequence, with 0, 1, 2, 3 denoting non-contrast, arterial, parenchymal and venous phase respectively. 648 randomly selected training sequences (Section III-A.1) were randomly split into 3 parts, each annotated by one operator. 141 testing sequences (Section III-A.2) were labelled by all three operators independently, and consensus were derived afterwards.

5) *DSA Atlas*: We selected 22 DSA sequences (12 AP and 10 lateral views) from 50 patients without stroke. Binary brain masks were delineated on those atlases for registration purposes as described in Section III-A.2.

IV. EXPERIMENTS AND RESULTS

A. Implementation

The proposed methods were implemented in Python. The deep learning model for phase classification was developed using Pytorch [34] on an NVIDIA 2080 Ti with 11 GB of memory. The deep learning network was trained with a batch size of 32 for 100 epochs. All training data were iterated once per epoch. To enrich the diversity of training set and prevent possible overfitting, the following augmentation techniques were randomly applied during data loading: horizontal flip, random rotate ($\in [-10^\circ, 10^\circ]$), random affine transformation (translation $\in [0, 0.1]$, scale $\in [0.8, 1.2]$). For this multi-class classification task, cross entropy was chosen as the loss function. We used the Adam optimizer [35] with an adaptive learning rate initialized at 0.001, halved every 10 epochs.

The parameters of the 2D Frangi filter [30] were optimized based on visual inspection ($\alpha = 0.5$, $\beta = 0.5$, $\gamma = 15$, $\sigma_{min} = 2$, $\sigma_{max} = 12$, $scale\ step = 2$). An intensity threshold of 0.08 was applied on filter output to segment vessel structures.

Motion correction and MINIP registration were performed using the SimpleElastix toolbox [36]. We chose affine transformation with advanced mattes mutual information [29] as the similarity metric and adaptive stochastic gradient descent (ASGD) [37] as the optimizer. The atlas mask was used as the moving image mask when registering atlases to post-EVT images. The parameter file used in this work can be found at <http://elastix.bigr.nl/wiki/index.php/Par0062>.

B. Evaluating Phase Separation

In the evaluation of phase separation, we assessed the added value of data augmentation, temporal information and the handcrafted constrained transition matrix module via an ablation study. In addition, we compared the method with inter-observer variability among three human annotators.

1) *Evaluation metrics*: The following metrics were adopted in this experiment:

- **average accuracy** represents the percentage of correctly classified images out of all the images;
- **weighted F1 score** refers to the harmonic mean of the precision and recall. In a multi-class problem of N_c classes, the weighted F1 ($F1_w$) is an average of F1 scores ($F1_i$) weighted by the number of images (S_i) from each class, as in Eq. 4:

$$F1_w = \frac{\sum_{i=1}^{N_c} S_i F1_i}{\sum_{i=1}^{N_c} S_i} \quad ; \quad (4)$$

- **frame offset** measures the phase separation accuracy on sequence level, rather than image level. The phase border frame index offset between classified and ground truth can serve as an insightful metric for phase separation accuracy. In this experiment, the average and standard deviation for offset of first, last arterial phase frame and last parenchymal phase frame were evaluated.

2) *Ablation Study*: Ablation experiments were performed to assess the contribution of separate components of the proposed algorithm. Table II summarizes the comparison under the aforementioned metrics. In all ablated cases, the model performance degraded. Without data augmentation, the generalizability of the model was reduced as a result of overfitting on the training data. Without incorporating neighboring frames as temporal information, the overall image level accuracy slightly dropped. The most marginal deterioration was observed at arterial/parenchymal border frame accuracy (51% vs 46%). Not surprisingly, by embedding human defined logic into the model, an overall performance improvement was evidenced across all metrics in the Table. More importantly, such a constrained transform matrix enforces phase transition logic within a sequence, suppressing unreasonable prediction errors.

3) *Inter-observer Variability*: Smooth transition between phases is often observed, which attributes to inter-observer variability during phase annotation. In this section, the algorithm variability is compared with three human annotators on the selected 141 sequences in test set. We computed the agreements in pairs for all combinations among the proposed method and three human annotators. For the agreement between the method and human annotators is defined as the average agreement between the method and each of the annotators. The inter-observer agreement is calculated as the average agreement among all human annotator pairs. As shown in Table II, the proposed method exhibits even better agreement than the inter-observer agreement, achieving human level annotation precision with robustness.

TABLE II: Performance overview of phase classification. Ablation study was performed with 5-fold cross validation on the training and validation set. Performance comparison with human annotator was assessed on the test set.

Method		Frame level metrics		Sequence level metrics								
		Average accuracy	Weighted F1	first arterial			last arterial			last parenchymal		
				acc	mean offset	std offset	acc	mean offset	std offset	acc	mean offset	std offset
Ablation	Proposed	0.92	0.92	0.92	0.10	0.41	0.51	0.70	1.20	0.66	0.42	0.84
	No augmentation	0.88	0.88	0.84	0.21	0.67	0.39	1.00	1.56	0.60	0.53	0.98
	No temporal info	0.91	0.91	0.91	0.12	0.47	0.46	0.76	1.23	0.66	0.43	0.84
	No state-transition matrix	0.91	0.91	0.91	0.14	0.55	0.51	0.89	3.21	0.66	0.49	1.41
Test	Method to observer agreement	0.90	0.90	0.88	0.14	0.48	0.34	1.10	1.54	0.55	0.63	1.11
	Observer to observer agreement	0.89	0.89	0.87	0.18	0.59	0.31	1.16	1.56	0.52	0.68	1.10

C. Evaluating autoTICI Quantification

In this section, the accuracy of autoTICI is evaluated based on the correlation with eTICI. Furthermore, we assessed the clinical value of autoTICI in comparison to eTICI with respect to mRS and NIHSS.

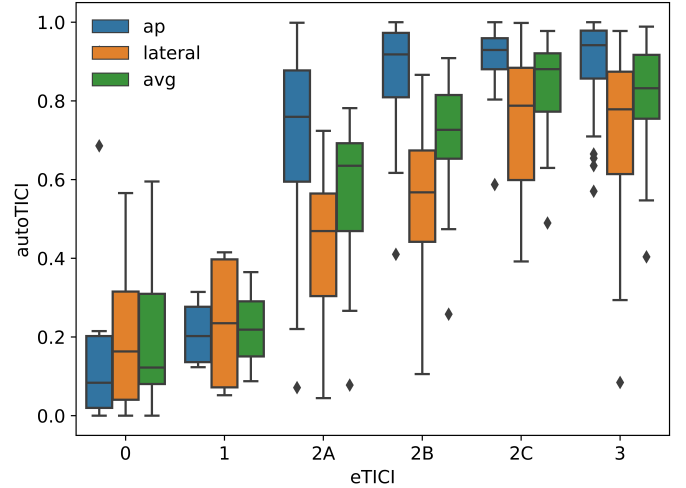
1) *autoTICI vs eTICI*: Fig. 7a shows the distribution of the proposed autoTICI versus eTICI on the test dataset. Spearman correlation test showed that both AP and lateral view autoTICI scores were significantly associated with eTICI with $\rho = 0.54$, ($P < 0.001$) and $\rho = 0.65$, ($P < 0.001$), respectively. The stronger correlation with lateral view autoTICI scores matches the expectation of clinical experts because the brain area in AP views is about half as in lateral projections and occlusion effects are generally better visualized in lateral view. Note that eTICI 2C and 3 are hard to distinguish for autoTICI, as both eTICI scores indicate nearly complete reperfusion.

We performed multinomial logistic regression between autoTICI and eTICI on the test data with leave-one-out cross validation. As shown in Fig. 7b, a micro-average (biased average by class frequency) AUC of 0.76 and 0.78 for AP and lateral view were achieved respectively. With both autoTICI scores as input features, the micro-average AUC reached 0.81. For dichotomized eTICI (failure: $\leq 2A$; success: $\geq 2B$), autoTICI achieved an AUC of 0.90.

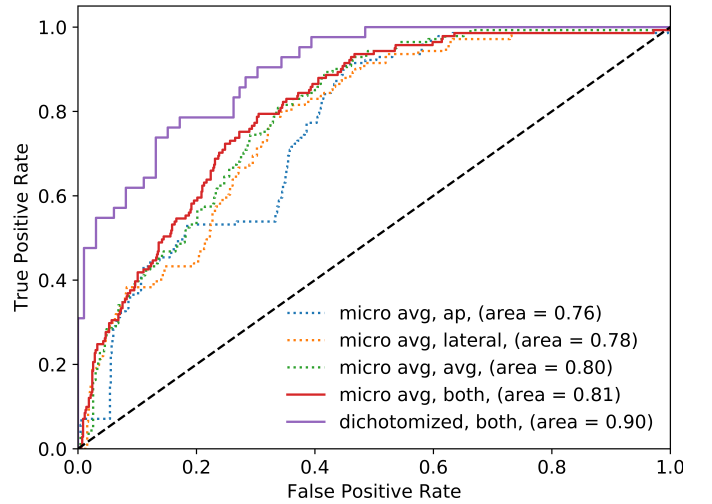
2) *Correlation to Treatment Outcome*: We further compared autoTICI and eTICI with respect to their correlation to treatment outcome in terms of mRS (III-B.2) and NIHSS (III-B.3). We used both AP and lateral autoTICI scores as input features for logistic regression. As shown in Fig. 8, cross validated logistic regression between TICI scores and mRS showed that autoTICI had a slightly higher AUC of 0.63 than 0.60 for eTICI. Similarly, the accuracy of autoTICI and eTICI were 0.66 and 0.62, respectively. Spearman correlation test was applied between TICI scores and NIHSS shift scores, which showed that autoTICI and eTICI were comparable with $\rho = 0.29$ ($P < 0.01$) and $\rho = 0.30$ ($P < 0.01$), respectively. Overall, autoTICI was on par with eTICI on outcome predictability.

TABLE III: autoTICI vs eTICI in terms of correlation to outcome.

Method	logistic regression			spearman correlation			
	dichotomized mRS			NIHSS.FU		NIHSS.shift	
	acc	AUC	odds ratio	ρ	P-value	ρ	P-value
autoTICI	0.66	0.63	1.27	-0.25	<0.01	0.29	<0.01
eTICI	0.62	0.60	1.02	-0.28	<0.01	0.30	<0.01



(a) autoTICI distribution with respect to eTICI. Blue: AP score; orange: lateral score; green: average of AP and lateral scores.



(b) Logistic regression ROC. Green, orange, blue, red: micro-average ROC of all eTICI grades; purple: dichotomized eTICI (failure: $\leq 2A$; success: $\geq 2B$).

Fig. 7: Correlation between autoTICI and eTICI.

V. DISCUSSION

We have presented a fully automatic, quantitative and truly perfusion based TICI scoring method that is inspired by traditional visual TICI assessment procedures. We exploited convolutional neural networks to tackle the phase separation challenge; it achieved performance on par with human experts. On the MR CLEAN registry, we demonstrated that

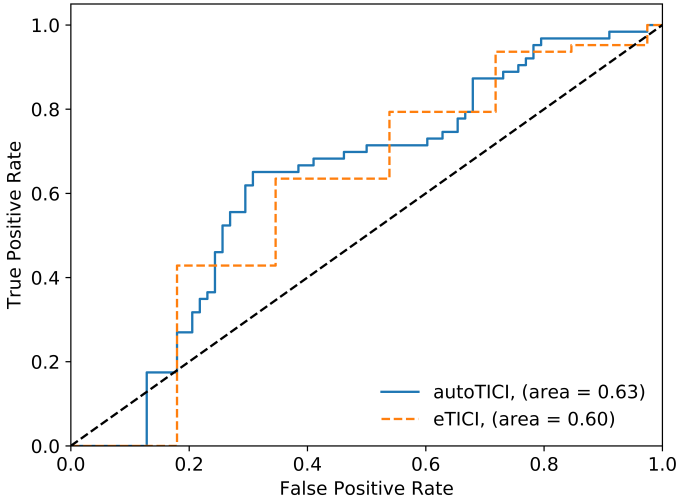


Fig. 8: Prediction of treatment outcome (mRS) using autoTICI.

the proposed autoTICI and eTICI are statistically significantly associated and they are both comparable predictors of functional outcome, revealing the potential value of autoTICI as a computer-aided biomarker for peri-procedural treatment assessment.

The proposed CNN based phase separation method demonstrated human-level precision. When considering prior-art, only Schuldhaus *et al.* [25] reported a quantitative performance results. On 14 DSA sequences, Schuldhaus *et al.* [25] reported 93% and 50% accuracy on first arterial border match and last arterial border match respectively. Accordingly, our proposed method achieved 92% and 51% respectively over 648 sequences. A pure numerical comparison seems to show comparable performance, but our study has different characteristics. It was tested on 648 instead of 14 sequences, these sequences originate from a multi-center registry, and the frame rates (2-4/fps) are higher than those (0.5-2/fps) reported by Schuldhaus *et al.* [25], and our approach also separates the venous phase.

Affine registration was performed during sequence alignment and atlas matching. In this work, all obtained DSA sequences were already subtracted during acquisition and the original masks were not always stored. In case of displacement between the original mask and its following frames, the subtraction action would introduce some undesired artifacts to the image, which are not trivial to fix by means of registration or other post-processing techniques. Besides, due to lacking of background texture, the registration relies on the skull outline and brain vasculature. The skull skeleton shown in a subtracted image is in fact an artifact of imperfect subtraction. Therefore, if the original non-subtracted images could be used instead, which encompass richer and more robust textural information, the registration accuracy could be potentially improved.

It must be pointed out that the proposed autoTICI is not equivalent to eTICI in terms of definition. While autoTICI focuses on brain tissue antegrade reperfusion quantification, eTICI also considers evidence of vessel revascularization and slow blood flow. In case of minimal reperfusion, eTICI distinguishes score 1 from 0 by judging whether antegrade

reperfusion has passed the initial occlusion. In case of (nearly) complete perfusion, eTICI emphasizes the existence of distal slow flow when comparing eTICI 2C to 3. Therefore, it would be inaccurate to linearly map autoTICI scores to the 6-grade eTICI scales. That is to say, the accuracy of autoTICI cannot be fully benchmarked by its correlation with eTICI.

End-to-end deep learning based methods might be valid alternatives to the automatic TICI scoring method proposed in this study. The reasons that we opted for a step-by-step strategy are (i) data: end-to-end training approaches treat all four sequences of each patient as one input data sample. Such methods generally require larger number of patients, as well as more sophisticated GPU resources; (ii) interpretability: while aiming for minimizing prediction errors, end-to-end training approaches generally sacrifices causal interpretability. The proposed method, by contrast, provides intermediate visualizable outputs per step, offering enriched clinical insights; (iii) quantitativity: rather than categorical TICI grading, we seek quantitative brain reperfusion analysis methods. Training end-to-end networks for this purpose is not straightforward due to lacking of quantitative ground truth.

From the clinical perspective, the proposed autoTICI provides an objective, reproducible and quantitative measure of EVT quality, eliminating human errors and variations. As it is a true measure of tissue level reperfusion, human conceptual confusion is avoided. Therefore, autoTICI overcomes the aforementioned three shortcomings of existing TICI scores. Moreover, such an automatic algorithm can be potentially integrated in clinical routines, such that an autoTICI scoring is automatically derived from each DSA run, which would support real-time peri-procedural decision making.

This is especially interesting in patients with futile recanalization, defined as patients with a technically successful EVT procedure with TICI 3 recanalization, and despite this a poor functional outcome, which has been reported in approx. 50 percent of TICI 3 patients [38]. This poor functional outcome can nowadays not be predicted by a human observer based on the completion DSA with the conventional eTICI scoring. Future application of our method potentially identifies these patients already at the end of the EVT procedure when additional drugs could be given or the treatment regimen could be altered to improve functional outcome.

VI. CONCLUSION

We presented a robust and fully automatic perfusion quantification method, autoTICI. On a large routinely acquired multi-center dataset, we have demonstrated that autoTICI is significantly correlated with the eTICI reference and possesses comparable treatment outcome predictive value, revealing its potential in future studies and clinical practice.

ACKNOWLEDGMENT

The authors would like to thank Kars C.J. Compagne for his assistance in patient data imputation.

REFERENCES

- [1] G. WHO, "Global health estimates 2016: deaths by cause, age, sex, by country and by region, 2000–2016," 2018.
- [2] R. T. Higashida and A. J. Furlan, "Trial design and reporting standards for intra-arterial cerebral thrombolysis for acute ischemic stroke," *Stroke*, vol. 34, no. 8, pp. e109–e137, 2003.
- [3] M. Goyal, B. K. Menon, W. H. van Zwam, D. W. Dippel, P. J. Mitchell, A. M. Demchuk, A. Dávalos, C. B. Majoie, A. Van Der Lugt, M. A. De Miquel *et al.*, "Endovascular thrombectomy after large-vessel ischaemic stroke: a meta-analysis of individual patient data from five randomised trials," *The Lancet*, vol. 387, no. 10029, pp. 1723–1731, 2016.
- [4] O. A. Berkhemer, P. S. Fransen, D. Beumer, L. A. Van Den Berg, H. F. Lingsma, A. J. Yoo, W. J. Schonewille, J. A. Vos, P. J. Nederkoorn, M. J. Wermer *et al.*, "A randomized trial of intraarterial treatment for acute ischemic stroke," *n Engl J Med*, vol. 372, pp. 11–20, 2015.
- [5] D. C. Haussen, S. Dehkharghani, S. Rangaraju, L. C. Rebello, M. Bouslama, J. A. Grossberg, A. Anderson, S. Belagaje, M. Frankel, and R. G. Nogueira, "Automated ct perfusion ischemic core volume and noncontrast ct aspects (alberta stroke program early ct score) correlation and clinical outcome prediction in large vessel stroke," *Stroke*, vol. 47, no. 9, pp. 2318–2322, 2016.
- [6] E. Venema, M. J. Mulder, B. Roozenbeek, J. P. Broderick, S. D. Yeatts, P. Khatri, O. A. Berkhemer, B. J. Emmer, Y. B. Roos, C. B. Majoie *et al.*, "Selection of patients for intra-arterial treatment for acute ischaemic stroke: development and validation of a clinical decision tool in two randomised trials," *bmj*, vol. 357, 2017.
- [7] C. Dargazanli, A. Consoli, M. Barral, J. Labreuche, H. Redjem, G. Ciccio, S. Smajda, J.-P. Desilles, G. Taylor, C. Preda *et al.*, "Impact of modified tici 3 versus modified tici 2b reperfusion score to predict good outcome following endovascular therapy," *American Journal of Neuroradiology*, vol. 38, no. 1, pp. 90–96, 2017.
- [8] J. Su, L. Wolff, A. C. M. van Es, W. van Zwam, C. Majoie, D. W. Dippel, A. van der Lugt, W. J. Niessen, and T. Van Walsum, "Automatic collateral scoring from 3d cta images," *IEEE Transactions on Medical Imaging*, vol. 39, no. 6, pp. 2190–2200, 2020.
- [9] D. Robben, A. M. Boers, H. A. Marquering, L. L. Langezaal, Y. B. Roos, R. J. van Oostenbrugge, W. H. van Zwam, D. W. Dippel, C. B. Majoie, A. van der Lugt *et al.*, "Prediction of final infarct volume from native ct perfusion and treatment parameters using deep learning," *Medical image analysis*, vol. 59, p. 101589, 2020.
- [10] I. I. T. Investigators, "The interventional management of stroke (ims) ii study," *Stroke*, vol. 38, no. 7, pp. 2127–2135, 2007.
- [11] M. A. Almekhlafi, S. Mishra, J. A. Desai, V. Nambiar, O. Volny, A. Goel, M. Eesa, A. M. Demchuk, B. K. Menon, and M. Goyal, "Not all 'successful' angiographic reperfusion patients are an equal validation of a modified tici scoring system," *Interventional Neuroradiology*, vol. 20, no. 1, pp. 21–27, 2014.
- [12] D. S. Liebeskind, S. Bracard, F. Guillemin, R. Jahan, T. G. Jovin, C. B. Majoie, P. J. Mitchell, A. van der Lugt, B. K. Menon, L. San Román *et al.*, "etici reperfusion: defining success in endovascular stroke therapy," *Journal of neurointerventional surgery*, vol. 11, no. 5, pp. 433–438, 2019.
- [13] O. O. Zaidat, A. J. Yoo, P. Khatri, T. A. Tomsick, R. Von Kummer, J. L. Saver, M. P. Marks, S. Prabhakaran, D. F. Kallmes, B.-F. M. Fitzsimmons *et al.*, "Recommendations on angiographic revascularization grading standards for acute ischemic stroke: a consensus statement," *Stroke*, vol. 44, no. 9, pp. 2650–2663, 2013.
- [14] G. Zhang, K. M. Treurniet, I. G. Jansen, B. J. Emmer, R. van den Berg, H. A. Marquering, M. Uyttenboogaart, S. F. Jenniskens, Y. B. Roos, P. J. van Doormaal *et al.*, "Operator versus core lab adjudication of reperfusion after endovascular treatment of acute ischemic stroke," *Stroke*, vol. 49, no. 10, pp. 2376–2382, 2018.
- [15] M. G. Lansberg, M. Straka, S. Kemp, M. Mlynash, L. R. Wechsler, T. G. Jovin, M. J. Wilder, H. L. Lutsep, T. J. Czartoski, R. A. Bernstein *et al.*, "Mri profile and response to endovascular reperfusion after stroke (defuse 2): a prospective cohort study," *The Lancet Neurology*, vol. 11, no. 10, pp. 860–867, 2012.
- [16] P. Khatri, J. Neff, J. P. Broderick, J. C. Khoury, J. Carrozella, and T. Tomsick, "Revascularization end points in stroke interventional trials: recanalization versus reperfusion in ims-i," *Stroke*, vol. 36, no. 11, pp. 2400–2403, 2005.
- [17] T. Tomsick, J. Broderick, J. Carrozella, P. Khatri, M. Hill, Y. Palesch, J. Khoury *et al.*, "Revascularization results in the interventional management of stroke ii trial," *American Journal of Neuroradiology*, vol. 29, no. 3, pp. 582–587, 2008.
- [18] A. J. Yoo, C. Z. Simonsen, S. Prabhakaran, Z. A. Chaudhry, M. Issa, J. E. Fugate, I. Linfante, D. F. Kallmes, G. Dabus, and O. O. Zaidat, "Refining angiographic biomarkers of reperfusion: modified tici is superior to tici for predicting clinical outcomes after intra-arterial therapy," 2013.
- [19] S. H. Suh, H. J. Cloft, J. E. Fugate, A. A. Rabinstein, D. S. Liebeskind, and D. F. Kallmes, "Clarifying differences among thrombolysis in cerebral infarction scale variants: is the artery half open or half closed?" *Stroke*, vol. 44, no. 4, pp. 1166–1168, 2013.
- [20] A. Nielsen, M. B. Hansen, A. Tietze, and K. Mouridsen, "Prediction of tissue outcome and assessment of treatment effect in acute ischemic stroke using deep learning," *Stroke*, vol. 49, no. 6, pp. 1394–1401, 2018.
- [21] R. McKinley, L. Häni, J. Gralla, M. El-Koussy, S. Bauer, M. Arnold, U. Fischer, S. Jung, K. Mattmann, M. Reyes *et al.*, "Fully automated stroke tissue estimation using random forest classifiers (faster)," *Journal of Cerebral Blood Flow & Metabolism*, vol. 37, pp. 2728–2741, 2017.
- [22] A. Liebeskind, A. Deshpande, J. Murakami, and F. Scalzo, "Automatic estimation of arterial input function in digital subtraction angiography," in *International Symposium on Visual Computing*. Springer, 2019, pp. 393–402.
- [23] H. Prasetya, L. A. Ramos, T. Epema, K. M. Treurniet, B. J. Emmer, I. R. Van Den Wijngaard, G. Zhang, M. Kappelhof, O. A. Berkhemer, A. J. Yoo *et al.*, "qtici: Quantitative assessment of brain tissue reperfusion on digital subtraction angiograms of acute ischemic stroke patients," *International Journal of Stroke*, p. 1747493020909632, 2020.
- [24] H.-J. Lee, J.-S. Hong, C.-J. Lin, Y.-H. Kao, F.-C. Chang, C.-B. Luo, and W.-F. Chu, "Automatic flow analysis of digital subtraction angiography using independent component analysis in patients with carotid stenosis," *PloS one*, vol. 12, no. 9, p. e0185330, 2017.
- [25] D. Schuldhaus, M. Spiegel, T. Redel, M. Polyanskaya, T. Struffert, J. Hornegger, and A. Doerfler, "Classification-based summation of cerebral digital subtraction angiography series for image post-processing algorithms," *Physics in Medicine & Biology*, vol. 56, p. 1791, 2011.
- [26] K. He, X. Zhang, S. Ren, and J. Sun, "Deep residual learning for image recognition," in *Proceedings of the IEEE conference on computer vision and pattern recognition*, 2016, pp. 770–778.
- [27] J. D. Lafferty, A. McCallum, and F. C. N. Pereira, "Conditional random fields: Probabilistic models for segmenting and labeling sequence data," in *Proceedings of the Eighteenth International Conference on Machine Learning*, ser. ICML '01, 2001, pp. 282–289.
- [28] G. D. Forney, "The viterbi algorithm," *Proceedings of the IEEE*, vol. 61, no. 3, pp. 268–278, 1973.
- [29] D. Mattes, D. R. Haynor, H. Vesselle, T. K. Lewellen, and W. Eubank, "Pet-ct image registration in the chest using free-form deformations," *IEEE transactions on medical imaging*, vol. 22, no. 1, pp. 120–128, 2003.
- [30] A. F. Frangi, W. J. Niessen, K. L. Vincken, and M. A. Viergever, "Multiscale vessel enhancement filtering," in *International Conference on Medical Image Computing and Computer-assisted Intervention*. Springer, 1998, pp. 130–137.
- [31] N. Otsu, "A threshold selection method from gray-level histograms," *IEEE transactions on systems, man, and cybernetics*, vol. 9, no. 1, pp. 62–66, 1979.
- [32] I. G. Jansen, M. J. Mulder, and R.-J. B. Goldhoorn, "Endovascular treatment for acute ischaemic stroke in routine clinical practice: prospective, observational cohort study (mr clean registry)," *bmj*, vol. 360, 2018.
- [33] M. J. Azur, E. A. Stuart, C. Frangakis, and P. J. Leaf, "Multiple imputation by chained equations: what is it and how does it work?" *International journal of methods in psychiatric research*, vol. 20, no. 1, pp. 40–49, 2011.
- [34] A. Paszke, S. Gross, F. Massa, A. Lerer, J. Bradbury, G. Chanan, T. Killeen, Z. Lin, N. Gimelshein, L. Antiga *et al.*, "Pytorch: An imperative style, high-performance deep learning library," in *Advances in neural information processing systems*, 2019, pp. 8026–8037.
- [35] D. P. Kingma and J. Ba, "Adam: A method for stochastic optimization," *arXiv preprint arXiv:1412.6980*, 2014.
- [36] K. Marstal, F. Berendsen, M. Staring, and S. Klein, "Simpleelastix: A user-friendly, multi-lingual library for medical image registration," in *Proceedings of the IEEE conference on computer vision and pattern recognition workshops*, 2016, pp. 134–142.
- [37] S. Klein, J. P. Pluim, M. Staring, and M. A. Viergever, "Adaptive stochastic gradient descent optimisation for image registration," *International journal of computer vision*, vol. 81, no. 3, p. 227, 2009.
- [38] N. van Horn, H. Knip, H. Leischner, R. McDonough, M. Deb-Chatterji, G. Broocks, G. Thomalla, C. Brekenfeld, J. Fiehler, U. Hanning *et al.*, "Predictors of poor clinical outcome despite complete reperfusion in acute ischemic stroke patients," *Journal of NeuroInterventional Surgery*, 2020.